

Endochondral bone in an Early Devonian 'placoderm' from Mongolia

Brazeau, Martin D.; Giles, Sam; Dearden, Richard P.; Jerve, Anna; Ariunchimeg, Ya.; Zorig, E.; Sansom, Robert; Guillaume, Thomas; Castiello, Marco

DOI:

[10.1038/s41559-020-01290-2](https://doi.org/10.1038/s41559-020-01290-2)

License:

Other (please specify with Rights Statement)

Document Version

Peer reviewed version

Citation for published version (Harvard):

Brazeau, MD, Giles, S, Dearden, RP, Jerve, A, Ariunchimeg, Y, Zorig, E, Sansom, R, Guillaume, T & Castiello, M 2020, 'Endochondral bone in an Early Devonian 'placoderm' from Mongolia', *Nature Ecology and Evolution*, vol. 4, no. 11, pp. 1477-1484. <https://doi.org/10.1038/s41559-020-01290-2>

[Link to publication on Research at Birmingham portal](#)

Publisher Rights Statement:

This document is the Author Accepted Manuscript version of a published work which appears in its final form in *Nature Ecology and Evolution*. The final Version of Record can be found at: <https://doi.org/10.1038/s41559-020-01290-2>

Subject to Springer Nature re-use terms: <https://www.nature.com/nature-research/editorial-policies/self-archiving-and-license-to-publish#terms-for-use>

General rights

Unless a licence is specified above, all rights (including copyright and moral rights) in this document are retained by the authors and/or the copyright holders. The express permission of the copyright holder must be obtained for any use of this material other than for purposes permitted by law.

- Users may freely distribute the URL that is used to identify this publication.
- Users may download and/or print one copy of the publication from the University of Birmingham research portal for the purpose of private study or non-commercial research.
- User may use extracts from the document in line with the concept of 'fair dealing' under the Copyright, Designs and Patents Act 1988 (?)
- Users may not further distribute the material nor use it for the purposes of commercial gain.

Where a licence is displayed above, please note the terms and conditions of the licence govern your use of this document.

When citing, please reference the published version.

Take down policy

While the University of Birmingham exercises care and attention in making items available there are rare occasions when an item has been uploaded in error or has been deemed to be commercially or otherwise sensitive.

If you believe that this is the case for this document, please contact UBIRA@lists.bham.ac.uk providing details and we will remove access to the work immediately and investigate.

Endochondral bone in an Early Devonian ‘placoderm’ from Mongolia

Martin D. Brazeau^{1,2*}, Sam Giles^{2,3,4}, Richard P. Dearden^{1,5}, Anna Jerve^{1,6}, Y.A.

Ariunchimeg⁷, E. Zorig⁸, Robert Sansom⁹, Thomas Guillaume¹⁰, Marco Castiello¹

¹ *Department of Life Sciences, Imperial College London, Silwood Park Campus, Buckhurst Rd, Ascot, SL5 7PY, UK;*

² *Department of Earth Sciences, Natural History Museum, Cromwell Road, London SW7 5BD, UK;*

³ *School of Geography, Earth and Environmental Sciences, University of Birmingham, Birmingham, UK;*

⁴ *Department of Earth Sciences, University of Oxford, South Parks Road, Oxford, OX1 3AN, UK;*

⁵ *CR2P Centre de Recherche en Paléontologie – Paris, Muséum national d’Histoire naturelle, Sorbonne Universités, CNRS, CP 38, 57 Rue Cuvier, 75231, Paris, Cedex 05, France*

⁶ *Department of Organismal Biology, Subdepartment of Evolution and Development, Uppsala University, Norbyvägen 18A, 752 36 Uppsala, Sweden;*

⁷ *Natural History Museum, P.O. Box 46/52, Ulaanbaatar 1420, Mongolia*

⁸ *Institute of Paleontology, Mongolian Academy of Science, P.O. Box 46/650, S. Danzan Street 3/1, Chingeltei District. Ulaanbaatar 15160, Mongolia;*

⁹ *School of Earth and Environmental Sciences, University of Manchester, Manchester M13 9PT, UK;*

¹⁰ *Department of Animal and Plant Sciences, The University of Sheffield, Sheffield S10 2TN, UK;*

26

27 * Author for correspondence.

Endochondral bone is the main internal skeletal tissue of nearly all osteichthyans—the group comprising more than 60,000 living species of bony fishes and tetrapods. Chondrichthyans (sharks and their kin) are the living sister group of osteichthyans and have cartilaginous endoskeletons, long considered the ancestral condition for all jawed vertebrates (gnathostomes). The absence of bone in modern jawless fishes and the absence of endochondral ossification in early fossil gnathostomes appears to lend support to this conclusion. Here we report the discovery of extensive endochondral bone in *Minjinia turgenensis*, a new genus and species of ‘placoderm’-like fish from the Early Devonian (Pragian) of western Mongolia described using x-ray computed microtomography (XR- μ CT). The fossil consists of a partial skull roof and braincase with anatomical details providing strong evidence of placement in the gnathostome stem group. However, its endochondral space is filled with an extensive network of fine trabeculae resembling the endochondral bone of osteichthyans. Phylogenetic analyses place this new taxon as a proximate sister group of the gnathostome crown. These results provide direct support for theories of generalised bone loss in chondrichthyans. Furthermore, they revive theories of a phylogenetically deeper origin of endochondral bone and its absence in chondrichthyans as a secondary condition.

The vertebrate skeleton comprises two main systems: the exoskeleton (external achondral dermal bones) and endoskeleton (internal chondral bones and cartilages, as well as some intramembranous bones)¹. An ossified exoskeleton evolved at least 450 million years ago in jawless stem gnathostomes^{2,3}, but the endoskeleton in these taxa is not endochondrally ossified. Endochondral bone, in which the cartilaginous endoskeletal precursor is invaded by and eventually replaced by bone, is widely considered an osteichthyan apomorphy³⁻⁷ and such a reliable identifying character gives the group its name. Extant chondrichthyans lack

dermal bone and possess a mainly cartilaginous endoskeleton enveloped by a structurally diverse range of tessellate calcified cartilage⁸. Outgroups of the gnathostome crown also lack endochondral ossification. Galeaspid surround their cartilaginous skeleton in globular calcified cartilage{NianZhong:2005tj}, while osteostracan and ‘placoderm’ endoskeletons were sheathed in perichondral bone³. Consequently, the last common ancestor of jawed vertebrates was long thought to have been perichondrally ossified, but lacking endochondral ossification³.

In this paper, we describe a new genus and species of ‘placoderm’ from the Early Devonian of western Mongolia. Although Mongolia is known for some of the geologically oldest putative gnathostome fossils (isolated chondrichthyan-like scales⁹⁻¹²), it remains a poorly sampled region of the world with respect to early vertebrates. ‘Placoderms’ were until now known from only a single fragmentary occurrence¹³ in the early Middle Devonian (Eifelian). Our new data highlight the importance of Mongolia as a key region for studies of early gnathostome evolution. We describe a braincase and partial skull roof representing the first substantial body fossil of an early gnathostome from Mongolia and displaying an unexpected occurrence of endochondral bone analysed using XR- μ CT. We conducted phylogenetic analyses to reconstruct the evolutionary relationships of this new taxon. To explore the evolutionary history of endochondral bone in light of this new discovery, we used parsimony and maximum likelihood ancestral states reconstruction. Finally, we discuss these results in the context of earlier statements about endochondral bone in non-osteichthyans, new developments in understanding the complexity and diversity of chondrichthyan endoskeletal tissues, and current uncertainties about early gnathostome phylogenetic relationships.

Systematic palaeontology

Gnathostomata Gegenbaur, 1874¹⁴

Minjinia turgenensis gen. et sp. nov.

Etymology. Generic name honours the memory of Chuluun Minjin for his extensive contributions to the Palaeozoic stratigraphy of Mongolia, his enthusiastic support of this work, and introducing us to the Yamaat River locality. Specific name recognises the provenance of the fossil from the Turgen region, Uvs aimag of western Mongolia.

Holotype. Institute of Paleontology, Mongolian Academy of Sciences MPC-FH100/9.1, a partial braincase and skull roof.

Type locality. Turgen Strictly Protected Area, Uvs province, western Mongolia; near the top of the stratigraphic sequence that occurs between the Tsagaan-Salaat and Yamaat Rivers.

Formation and age. Upper part of Tsagaansalaat Formation, Pragian (Early Devonian) ^{15,16}.

Diagnosis. ‘Placoderm’-grade stem gnathostome with endochondral bone, deep epaxial muscle cavities flanking a slender occipital ridge, and the following possible autapomorphies: dermal bones covered in sparsely placed tubercles, penultimate spino-occipital nerve canal substantially larger in diameter than others.

Description

MPC-FH100/9.1 consists of a partial braincase and skull roof (Fig. 1). The skull roof is ornamented with sparsely distributed finely ridged tubercles resembling those of the Siberian ‘placoderm’ *Dolganosteus*¹⁷; the tubercles become more broadly separated towards the

midline of the skull. They are distinct from those of *Dolganosteus* in that towards the midline of the skull roof, the tubercles are larger and more pointed. The specimen shows signs of extensive post-mortem transport, with angles of the braincase worn off and much of the skull roof and some of the braincase preserved as a mould. Individual skull roof ossifications cannot be identified, although this may be due to the dominantly mouldic preservation. There appears to have been a prominent nuchal plate eminence comparable to certain acanthothoracids such as *Romundina*¹⁸ and *Arabosteus*¹⁹.

Endoskeletal tissue. The braincase of MPC-FH100/9.1 is well ossified, comprising an external bony sheath filled with an extensive matrix of spongy tissue (Fig. 2a-b; Extended Data Fig. 1; Supplementary Video 1). The trabecles forming this tissue are irregular and branching, less than 1 mm thick and often curved, and resemble most closely the endochondral tissue of osteichthyans (Fig. 2c-d; Supplementary Video 2). As such, we interpret this as endochondral bone. Notably, this is found in all preserved regions of the braincase, in contrast to the isolated trabeculae previously identified as endochondral bone in *Boreaspis*²⁰ and *Bothriolepis*²¹. The margins of the braincase, the endocranial walls, and the boundaries of nerve and blood canals, are formed from a thicker tissue which we interpret as perichondral bone. This suggests that the endoskeleton of *Minjinia* comprises osteichthyan-like endochondral bone, with an ossified perichondrium. To address the possible alternative explanation that it is an aberrant instance of calcified cartilage, we compared the structure of this tissue with rarely-preserved mineralized cartilage in the stem chondrichthyan *Diplacanthus crassismus* (National Museums of Scotland specimen NMS 1891.92.334; Fig. 2e-f) observed using synchrotron tomography. The cancellae within the endochondral tissue of *Minjinia* are irregular, with a diameter of approximately 1-2 mm. This tissue is distinctly

unlike the calcified cartilage of *Diplacanthus* in appearance, which consists of a densely packed matrix of irregularly stacked chondrons between 20-60 µm in diameter.

Neurocranium. The braincase is preserved from the level of the right posterior orbital wall to the posterior end of the occipital ridge. Occipital glenoid condyles are not preserved, but much of the rest of the broad, flat parachordal region is present, separated by a midline groove that accommodated a relatively narrow notochordal tunnel. An asymmetric transverse fissure spans the basicranial surface at about mid-length of the preserved portion. It appears to demarcate the anterior margin of the parachordal plates and may correspond to the ventral cranial fissure of crown-group gnathostomes. However, unlike in crown gnathostomes, it is traversed by a substantial anterior extension of the cranial notochord. The courses of the lateral dorsal aortae are marked by a pair of sulci on the lateral margins of the parachordal plates, though only a short part of the canal is preserved on the right side of the specimen. A narrow, shallow sulcus for the efferent hyoid artery is present on the preserved right side of the specimen, immediately behind the level of the orbit (Fig. 1a).

The lateral surface of the braincase is preserved on the right side as a mouldic impression in the matrix (Fig. 1). A sharply demarcated hyoid fossa is present on the lateral wall of the otic region (Fig. 1). Posterior to this, a stout but pronounced vagal process with a pair of rounded eminences likely corresponds to the branchial arch articulations. There is no evidence for a pair of anterior and posterior divisions to the vagal process, which are typically seen in other ‘placoderms’. A well-developed ‘placoderm’-like craniospinal process is absent; its homologous position is instead covered in perichondral bone and marked by a low ridge (Fig. 1).

In posterior view, a tall, narrow median occipital ridge is evident and resembles the morphology of *Romundina*²² and *Arabosteus*¹⁹. Similar to these taxa, the median otic ridge is

152 flanked by two large occipital fossae for the epaxial musculature. The notochordal tunnel is
153 approximately the same size as or smaller than the foramen magnum, as in ‘placoderms’ and
154 in contrast with crown-group gnathostomes. A metotic fissure is absent.

155
156 **Endocast.** A partial cranial endocast is preserved, consisting of the hindbrain cavity, partial
157 midbrain cavity, labyrinth cavities, and posteromedial corner of the orbital region. The two
158 primary trunk canals of the trigeminal nerve (N.V₁ and N.V_{2,3}) are preserved (Fig. 3). The
159 acoustic (N.VIII) and facial nerve (N.VII) canals share a common trunk canal behind the
160 trigeminal nerves, as in many other ‘placoderms’²²⁻²⁵. The facial nerve canal branches into
161 palatal and hyomandibular branches between the saccular chamber and rear orbit wall (Fig. 3;
162 Extended Data Fig. 2), indicating this division was internal (deep) to the otic process. The
163 supraorbital branch opens into the rear wall of the orbit and part of its supraorbital
164 course is preserved (Fig. 3; Extended Data Fig. 2). A slender branch extends below the
165 labyrinth and divides into palatine and hyomandibular branches (Fig 3; Extended Data Fig.
166 2). As in other ‘placoderm’-grade taxa, the vagus nerve (N. X) trunk canal is very large in
167 diameter and exits from immediately behind the labyrinth cavity (Fig. 3). The spino-occipital
168 region resembles other ‘placoderms’ in being extended. At least four spino-occipital nerve
169 canals are present in a linear series, and the penultimate canal is largest in diameter (Fig. 3).
170 Intercalating these is a network of occipital artery canals branching from the dorsal aortae.

171 The skeletal labyrinth is not complete on either side of the specimen, but can mostly
172 be reconstructed according to the assumption of bilateral symmetry. The most significant
173 feature is that the labyrinth and endolymphatic cavity are joined to the main endocavity
174 chamber (Fig. 3). This is a striking contrast to other ‘placoderms’ and closely resembles
175 crown-group gnathostomes²⁶. The endolymphatic canals are elongate and tubular, extending
176 posterolaterally to reach the skull roof, though external openings cannot be clearly identified.

The anterior semi-circular canal follows the saccular cavity closely as in petalichthyids²⁷(Fig. 3). However, the horizontal and posterior canals appear to extend well away from the saccular chamber (Fig. 3). The dorsal junctions of the anterior and posterior canals are joined in a crus commune, as in *Romundina*²² and *Jagorina*²³. A sinus superior is absent.

Phylogenetic analyses

We conducted phylogenetic analyses under four different protocols: equal weights parsimony, implied weights parsimony, an unpartitioned Bayesian analysis, and a Bayesian analysis with characters partitioned by fit determined under implied weights parsimony²⁸ (see Extended Data Figs. 3-6). All phylogenetic analyses consistently place *Minjinia* as a stem-group gnathostome, proximate to the gnathostome crown (Fig. 4, Extended Data Figs 3, 4). *Minjinia* is recovered in a position crownward of arthrodires but outside of a grade consisting of *Entelognathus*, *Ramirosuarezia*, and *Janusiscus*. Under implied weights parsimony, these three taxa move onto the osteichthyan stem and *Minjinia* is placed as the immediate sister taxon of the gnathostome crown. Under parsimony, the crownward position of *Minjinia* is unambiguously supported by the skeletal labyrinth and endolymphatic duct being confluent with the main cranial cavity²⁶ (Supplementary Information). In common with arthrodires and the gnathostome crown²⁹, *Minjinia* possesses a division of the facial nerve(Fig. 3; Extended Data Fig. 2) deep to the transverse otic process. However, *Minjinia* is excluded from the gnathostome crown group due to the absences of a metotic fissure and a posterior dorsal fontanelle, and presence of broad, flat parachordal plates expanded behind the saccular cavity (Fig. 3, Supplementary Information).

We undertook ancestral states reconstructions to assess the evolutionary history of endochondral bone (Fig. 4; Extended Data Figs. 5 & 6; Supplementary Information).

Interestingly, parsimony analysis fails to recover secondary homology of this trait between

Minjinia and osteichthyans. The crownward placement of *Minjinia* is, in fact, based on independent evidence relating to anatomical features of the braincase and endocast. However, the resolution becomes ambiguous if missing data in either *Entelognathus* or *Ramirosuarezia* are resolved as having endochondral bone. The reconstruction becomes similarly ambiguous if *Janusiscus* is moved a single branch (requiring only two additional steps) onto the chondrichthyan stem. The strict precision of parsimony reconstructions makes it insensitive to this underlying uncertainty. To explore this, we used likelihood reconstructions and compared the ancestral state reconstructions under equal rates (ER) and all rates different (ARD) variants of the Mk_v model on branch-length-rescaled parsimony trees and Bayesian trees. Both models show substantial non-zero marginal likelihoods if endochondral bone is assumed present in the common node of *Minjinia* and Osteichthyes, with ARD strongly favouring its presence (0.33 for ER; 0.81 for ARD; Fig. 3, Table 1, Extended Data Figs. 5, 6, Supplementary Table 1). Under the ARD model, there is nearly equivocal support for presence or absence of endochondral bone at the gnathostome crown node (Table 1). The ARD model shows the best fit for endochondral bone (likelihood ratios 4.75 for parsimony [$p = 0.029$] and 5.26 for Bayesian, [$p = 0.022$]) (Table 1, Supplementary Table 1), favouring repeated losses of this tissue over multiple gains (see Discussion).

Discussion

Minjinia turgenensis presents an unexpected discovery of extensive endochondral bone in a ‘placoderm’-grade fish, with repercussions for the phylogenetic origin of this tissue and the problem of early gnathostome relationships more generally. The prevailing hypothesis has been that endochondral bone is an osteichthyan apomorphy^{3,7,29}. However, recent discoveries have cast doubt on this assertion. The recognition that dermal bone is secondarily lost in chondrichthyans^{30,31} (Fig. 4) is consonant with prior knowledge of the loss of perichondral

bone in this same lineage³². Taken together, this has revived uncertainty about the true phylogenetic timing of the origin of endochondral ossification³³. *Minjinia* provides direct corroboration for a more ancient origin.

Minjinia does not represent the first report of endochondral bone outside of Osteichthyes. However, it is by far the most extensive and unequivocal example and raises explicit questions in light of the proximity of *Minjinia* to the gnathostome crown (Fig. 4; Extended Data Figs. 3, 4). Isolated examples of trabecular endoskeletal bone have historically been reported in boreaspid osteostracans^{20,34}, a rhenanid³⁵, arthrodiros³⁶, a ptyctodont³⁷, and a petalichthyid^{38,39}. However, these reports are nearly all unillustrated statements; they have all been considered tenuous³ or dismissed as misidentifications⁵. In line with these assessments, we found no evidence of endochondral bone in material of *Buchanosteus* held in the Natural History Museum, London, or indeed in any other ‘placoderms’ we have examined. The *Epipetalichthys* holotype (Museum für Naturkunde, Berlin specimen MB.f.132.1-3) shows an apparently spongiose infilling in the anterior region of the braincase, but the identity of this structure, or even whether it is biological, cannot be determined. The *Epipetalichthys* tissue figured by Stensiö³⁸ was very superficial, and possibly represents the retreat of perichondral bone deposited during cartilage growth³⁹. Most recently, trabeculae in supposed endoskeletal pelvic bones of *Bothriolepis* have been termed endochondral bone²¹, although the small scale of these is in line with ‘superficial’ perichondral trabeculae seen elsewhere³⁸. The reported examples in boreaspid osteostracans have also been dismissed by later authors^{3,5}. Although they warrant further study, their tissue structures are unlikely to be homologous to osteichthyans owing to their phylogenetic remoteness and nested position in the Osteostraci⁴⁰.

Among chondrichthyans, endochondral bone has been mentioned in ‘acanthodians’^{3,41} and superficial bone-like tissues have been reported in the skeletons of extant

chondrichthyans. We are unable to substantiate statements about acanthodians: no authors have cited primary sources or specimens. One possible source is Watson's⁴² description of "massive ossification" of the endoskeleton of *Diplacanthus*. However, our synchrotron data of this same specimen (Fig. 2) shows that this tissue is undoubtably calcified cartilage. Some authors have speculated that the superficial mineralised tissue in the jaws of acanthodians or chondrichthyans may have developed in an endochondral position³⁹. Histological studies show that endoskeletal mineralization in the jaws of acanthodians is globular calcification and occasionally 'sub-tessellate'^{8,43}. Recent comparative histology and development in extant chondrichthyans has shown the presence of an extensive canalicular network in the tesserae⁴⁴ and a trabecular tesseral network in some vertebral elements⁴⁵, both resembling bone. Whether these represent homologues of osteichthyan examples remains open to debate; future works could employ synchrotron microtomography of stem-chondrichthyan cartilages to address these questions.

Does endochondral bone have a deep origin within the gnathostome stem group? This would imply repeated losses of this tissue. We do find statistical support for this hypothesis (Fig. 4, Table 1, Extended Data Figs. 5, 6, Supplementary Table 1), and the model is well justified on prior phylogenetic and biological grounds. Endochondral bone has long been known to be inconsistently developed across 'primitive' bony fishes: incomplete, polymorphic, or entirely absent ossification of the endoskeleton is known in both Palaeozoic actinopterygians^{41,46,47} and sarcopterygians {Cloutier:wm}, as well as more recent taxa⁴⁸. The frequent absence of endochondral bone in osteichthyans is considered secondary, and other controlling factors such as body size, maturity, mechanical stress, and buoyancy can determine its degree of development¹. Our findings are also in agreement with studies establishing a genetic basis for secondary loss of all bone types within chondrichthyans⁴⁹⁻⁵¹,

with the failure to produce endochondral bone likely representing arrested development of chondrocytes as opposed to a primary lack of ability⁵².

Another confounding factor in this question is the problem of ‘placoderm’ relationships. Although currently resolved in most analyses as a deeply pectinate grade along the gnathostome stem (Fig. 4), the backbone of this arrangement has poor statistical support, even in the present analysis (Extended Data Figs. 3). There is a lack of consistency in the arrangement of plesia and Bayesian tip-dating methods have even recovered a monophyletic Placodermi⁵³. *Minjinia* itself highlights this uncertainty, given its highly unexpected character combinations. Notwithstanding its endochondral bone and crown-gnathostome-like inner ear structure, it resembles ‘acanthothoracids’—the ‘placoderms’ widely considered among the most removed from the gnathostome crown (i.e. most ‘primitive’): it possesses deep epaxial fossae either side of a prominent occipital ridge and a nuchal eminence otherwise seen only in acanthothoracids such as *Romundina*¹⁸ and *Arabosteus*¹⁹. This apparent character conflict could perhaps be more easily reconciled with a more coherent (though not necessarily monophyletic) ‘placoderm’ assemblage. Indeed, the highly pectinate structure of the ‘placoderm’ grade seems symptomatic of an overemphasis on characters and taxa resembling the crown group, thereby undersampling characters that could stabilise a clear picture of ‘placoderm’ interrelationships.

Minjinia turgenensis reveals new data on ‘placoderm’ endoskeleton and tissue diversity recorded from Mongolia—an otherwise extremely poorly known biogeographic realm for early gnathostomes. The phylogenetic placement of this ‘acanthothoracid’-like taxon crownward of all non-maxillate ‘placoderms’, in conjunction with possession of extensive endochondral bone, highlights the importance of material from traditionally undersampled geographic areas. The presence of endochondral bone renews the hypothesis that this tissue is evolutionarily ancient and was lost secondarily in chondrichthyans^{6,33}. This

view is overall consistent with evidence of generalised bone loss in chondrichthyans, potentially as a result of the suppression of bone-generating molecular genetic pathways^{51,52}. Continued work in Mongolia and re-evaluation of phylogenetic datasets will be necessary to address this, with the results likely to lead to substantial re-evaluation of gnathostome phylogeny.

Methods

X-ray computed microtomography. We scanned MPC-FH100/9.1 using the Nikon XT 225s at the Museum of Paleontology, University of Michigan with the following parameters: 200kV, 140 μ A, over 3123 projections and a voxel size of 32.92 μ m. We conducted segmentation using Mimics 19.0 (<http://biomedical.materialise.com/mimics>; Materialise, Leuven, Belgium) and we imaged models for publication using Blender (<https://www.blender.org>).

Synchrotron light propagation phase contrast tomography. We imaged *Diplacanthus crassismus* specimen NMS 1891.92.334 on Beamline 19 of the European Synchrotron Radiation Facility, using propagation phase-contrast synchrotron microtomography. We performed a spot scan with an energy of 116keV, achieving a voxel size of 0.55 μ m. We processed the resulting tomograms using VG StudioMax 2.2 (Volume Graphics, Germany), and prepared images in Blender.

Phylogenetic analysis. We conducted a parsimony analysis using TNT 1.5⁵⁴ and Bayesian analysis using MrBayes v 3.2.7⁵⁵. The dataset consisted of 95 taxa and 284 discrete characters based on a pre-existing dataset⁵⁶. We employed Osteostraci and Galeaspida as composite outgroups. We conducted parsimony analysis using both equal weights and

implied weights methods. Global settings were 1000 search replicates and a hold of up to 1 million trees. Equal weights parsimony analyses were conducted using the ratchet with default settings. Implied weights parsimony used a concavity parameter of 3 and the search was without the ratchet. Command lists are included in Supplementary Information. We conducted Bayesian analysis using both a partitioned and unpartitioned dataset. We used the Mkv model⁵⁷ and gamma rate distribution. We ran the analyses for 5 million generations with a relative burn-in fraction of 0.25. Runs were checked for convergence using Tracer⁵⁸. We partitioned the dataset using a newly proposed method²⁸ that partitions the data according to homoplasy levels. Using the results of implied weights parsimony conducted in TNT, we created a text table of character fit values. We wrote an R⁵⁹ script to generate a list of partition commands for MrBayes.

We assessed parsimony ancestral states visually using Mesquite⁶⁰. Likelihood and Bayesian ancestral states were estimated in R using the castor package⁶¹ version 1.5.7. Prior to calculating likelihood ancestral states on parsimony trees, we scaled branch lengths using PAUP*⁶² and calculated the likelihood scores for all of the trees under the Mkv model with gamma rate parameter. The trees were then exported with branch lengths. To account for overall uncertainty in tree estimates, we estimated ancestral states on 100 trees randomly selected from the fundamental set of most parsimonious trees and two times 50 trees selected from the 75% last trees of each posterior tree distribution from the Bayesian analysis. We then run an ancestral states estimation Mk model (using the castor R package) using both the Equal Rates (ER) and All Rates Different (ARD) models. This resulted in 400 ancestral states estimations. For each estimation we extracted the overlap log likelihood, the AIC (counting one parameter for the ER model and two for the ARD model) and the scaled log likelihood (probability) for the presence and absence of the endochondral bone character (character 4) for the last common node of *Minjinia* and crown-group gnathostomes. We present the median

value of these distributions of the estimations overall log likelihoods, AICs and presence or absence of endochondral bone in Table 1.

Data availability

The holotype specimen of *Minjinia turgenensis* will be permanently deposited in the collections of the Institute of Paleontology, Mongolian Academy of Sciences. Original tomograms are available at (doi:10.6084/m9.figshare.12301229) and rendered models are available at (doi:10.6084/m9.figshare.12301223). The phylogenetic character list and dataset are available as Supplementary Information S1 and S2. The LifeScience Identifier for *Minjinia turgenensis* is urn:lsid:zoobank.org:act:82A1CEEC-B990-47FF-927A-D2F0B59AEA87

Code availability

R code for generating partitions based on character fits and code for likelihood ancestral states reconstructions and plots are available in the Supplementary Information.

References

1. Hall, B. K. *Bones and Cartilage*. (Academic Press, 2005).
2. Janvier, P. *Early Vertebrates*. (Oxford University Press, 1996).
3. Donoghue, P. C. J., Sansom, I. & Downs, J. P. Early evolution of vertebrate skeletal tissues and cellular interactions, and the canalization of skeletal development. *Journal of Experimental Zoology* **306B**, 278–294 (2006).
4. Rosen, D. E., Forey, P. L., Gardiner, B. G. & Patterson, C. Lungfishes, tetrapods, paleontology, and plesiomorphy. *Bull Am Mus Nat Hist* **167**, 159–276 (1981).

- 375 5. Gardiner, B. G. The relationships of the palaeoniscid fishes, a review based on new
376 specimens of *Mimia* and *Moythomasia* from Upper Devonian of Western Australia.
377 *Bull Br Mus nat Hist (Geol)* **37**, 173–428 (1984).
- 378 6. Maisey, J. G. Heads and tails: a chordate phylogeny. *Cladistics* **2**, 201–256 (1986).
- 379 7. Friedman, M. & Brazeau, M. A Reappraisal of the origin and basal radiation of the
380 Osteichthyes. *J Vertebr Paleontol* **30**, 36–56 (2010).
- 381 8. Maisey, J. G., Denton, J. S. S., Burrow, C. & Pradel, A. Architectural and
382 ultrastructural features of tessellated calcified cartilage in modern and extinct
383 chondrichthyan fishes. *Journal of Fish Biology* **15**, 37–23 (2020).
- 384 9. Karatajūtė-Talimaa, V. & Novitskaya, L. *Sodolepis*—a new representative of
385 Mongolepidida (Chondrichthyes?) from the lower Silurian of Mongolia.
386 *Paleontologicheskii Zhurnal* **5**, 96–103 (1997).
- 387 10. Karatajūtė-Talimaa, V. & Novitskaya, L. *Teslepis*—a new representative of
388 mongolepid elasmobranchs from the Lower Silurian of Mongolia. *Paleontologicheskii*
389 *Zhurnal* **4**, 36–43 (1992).
- 390 11. Karatajūtė-Talimaa, V., Novitskaya, L. & Rozman, K. S. *Mongolepis*—a new lower
391 Silurian genus of elasmobranchs from Mongolia. *Paleontologicheskii Zhurnal* **1**, 76–
392 86 (1990).
- 393 12. Andreev, P. *et al.* The systematics of the Mongolepidida (Chondrichthyes) and the
394 Ordovician origins of the clade. *PeerJ* **4**, e1850–e1850 (2016).
- 395 13. Vorobjeva, E. I. & Janvier, P. Observations to the note by E Vorobjeva: ‘First
396 discovery of Palaeozoic fishes on the territory of the Mongolian Republic’.
397 *Palaeontology and Biostratigraphy of Mongolia*, Moscow, 3, 134–136 (in Russian).
398 *Geobios* **17**, 379–380 (1984).

- 399 14. Gegenbaur, C. *Grundriss der vergleichenden Anatomie*. 1–680 (Wilhelm Engelmann,
400 1874).
- 401 15. Alekseeva, R. E., Mendbayar, B. & Erlanger, O. A. *Brachiopods and Biostratigraphy*
402 *of the Lower Devonian of Mongolia*. **16**, (Nauka, 1981).
- 403 16. Alekseeva, R. E. *Devonian Biostratigraphy of Mongolia*. (Nauka, 1993).
- 404 17. Mark-Kurik, E. in *Morphology, Phylogeny and Paleobiogeography of Fossil Fishes*
405 (eds. Elliott, D. K., Maisey, J., Yu, X. & Miao, D.) 101–106 (2010).
- 406 18. Ørvig, T. Description, with special reference to the dermal skeleton, of a new radotinid
407 arthrodire from the Gedinian of Arctic Canada. *Colloque international C.N.R.S. no.*
408 *218* 43–71 (1975).
- 409 19. Olive, S., Goujet, D., Lelièvre, H. & Janjou, D. A new Placoderm fish
410 (Acanthothoraci) from the Early Devonian Jauf Formation (Saudi Arabia).
411 *Geodiversitas* **33**, 393–409 (2011).
- 412 20. Wängsjö, G. The Downtonian and Devonian vertebrates of Spitsbergen. IX. *Norsk*
413 *Polarinstitut Skrifter* **97**, 1–611 (1952).
- 414 21. Charest, F., Johanson, Z. & Cloutier, R. Loss in the making: absence of pelvic fins and
415 presence of paedomorphic pelvic girdles in a Late Devonian antiarch placoderm
416 (jawed stem-gnathostome). *Biology Letters* **14**, 20180199 (2018).
- 417 22. Dupret, V., Sanchez, S., Goujet, D. & Ahlberg, P. E. The internal cranial anatomy of
418 *Romundina stellina* Ørvig, 1975 (Vertebrata, Placodermi, Acanthothoraci) and the
419 origin of jawed vertebrates—Anatomical atlas of a primitive gnathostome. *PLoS ONE*
420 **12**, e0171241 (2017).
- 421 23. Stensiö, E. A. La cavité labyrinthique, l’ossification sclérotique et l’orbite de *Jagorina*.
422 *Colloques internationaux du Centre national de la Recherche scientifique* **21**, 9–43
423 (1950).

- 424 24. Stensiö, E. A. Anatomical studies on the arthrodiran head. *K Sven Vetenskapsakad*
425 *Handl* **9**, 1–419 (1963).
- 426 25. Goujet, D. *Les poissons placodermes du Spitsberg*. (Cahiers de Paléontologie, Editions
427 du CNRS, 1984).
- 428 26. Davis, S. P., Finarelli, J. A. & Coates, M. I. *Acanthodes* and shark-like conditions in
429 the last common ancestor of modern gnathostomes. *Nature* **486**, 247–250 (2012).
- 430 27. Castiello, M. & Brazeau, M. D. Neurocranial anatomy of the petalichthyid placoderm
431 *Shearsbyaspis oepiki* Young revealed by X-ray computed microtomography.
432 *Palaeontology* **61**, 369–389 (2018).
- 433 28. Rosa, B. B., Melo, G. A. R. & Barbeitos, M. S. Homoplasy-based partitioning
434 outperforms alternatives in Bayesian analysis of discrete morphological data.
435 *Systematic Biology* **54**, 373 (2019).
- 436 29. Brazeau, M. D. & Friedman, M. The characters of Palaeozoic jawed vertebrates. *Zool*
437 *J Linn Soc* **170**, 779–821 (2014).
- 438 30. Zhu, M. *et al.* A Silurian placoderm with osteichthyan-like marginal jaw bones. *Nature*
439 **502**, 188–193 (2013).
- 440 31. Giles, S., Friedman, M. & Brazeau, M. D. Osteichthyan-like cranial conditions in an
441 Early Devonian stem gnathostome. *Nature* **520**, 82–85 (2015).
- 442 32. Miles, R. S. in *Interrelationships of Fishes* (eds. Greenwood, P. H., Miles, R. S. &
443 Patterson, C.) 63–103 (Academic Press London, 1973).
- 444 33. Zhu, M. Bone gain and loss: insights from genomes and fossils. *Natl Sci Rev* **1**, 490–
445 492 (2014).
- 446 34. Janvier, P. *Les céphalaspides du Spitsberg*. (Éditions du Centre National de la
447 Recherche Scientifique, 1985).

- 448 35. Ørvig, T. Histologic studies of placoderms and fossil elasmobranchs. *Arkiv för Zoologi*
449 **2**, 321–454 (1951).
- 450 36. Young, G. C. New information on the structure and relationships of *Buchanosteus*
451 (Placodermi: Euarthrodira) from the Early Devonian of New South Wales. *Zool J Linn*
452 *Soc* **66**, 309–352 (1979).
- 453 37. Miles, R. S. & Young, G. C. in *Problems in Vertebrate Evolution* (eds. Andrews, S.
454 M., Miles, R. S. & Walker, A. D.) 123–198 (Academic Press, 1977).
- 455 38. Stensiö, E. A. On the head of the macropetalichthyids. *Field Museum of Natural*
456 *History Publication Geological Series* **4**, 87–197 (1925).
- 457 39. Ørvig, T. Notes on some Paleozoic lower vertebrates from Spitsbergen and North
458 America. *Norsk Geologisk Tidsskrift* **37**, 285–353 (1957).
- 459 40. Sansom, R. Phylogeny, classification and character polarity of the Osteostraci
460 (Vertebrata). *Journal of Systematic Palaeontology* **7**, 95–115 (2009).
- 461 41. Schaeffer, B. The braincase of the holostean fish *Macrepistius*, with comments on
462 neurocranial ossification in the Actinopterygii. *American Museum Novitates* **2459**, 1–
463 34 (1971).
- 464 42. Watson, D. M. S. The acanthodian fishes. *Philosophical Transactions of the Royal*
465 *Society of London. Series B, Biological Sciences* **228**, 49–146 (1937).
- 466 43. Burrow, C. J., Davidson, R. G., Blaauwen, den, J. L. & Newman, M. J. Revision of
467 *Climatius reticulatus* Agassiz, 1844 (Acanthodii, Climatiidae), from the Lower
468 Devonian of Scotland, based on new histological and morphological data. *J Vertebr*
469 *Paleontol* **35**, e913421 (2015).
- 470 44. Dean, M. N., Socha, J. J., Hall, B. K. & Summers, A. P. Canaliculi in the tessellated
471 skeleton of cartilaginous fishes. *Journal of Applied Ichthyology* **26**, 263–267 (2010).

- 472 45. Atake, O. J., Cooper, D. M. L. & Eames, B. F. Bone-like features in skate suggest a
473 novel elasmobranch synapomorphy and deep homology of trabecular mineralization
474 patterns. *Acta Biomaterialia* **84**, 424–436 (2019).
- 475 46. Pearson, D. M. & Westoll, T. S. The Devonian actinopterygian *Cheirolepis* Agassiz.
476 *Transactions of the Royal Society of Edinburgh: Earth Sciences* **70**, 337–399 (1979).
- 477 47. Giles, S. *et al.* Endoskeletal structure in *Cheirolepis* (Osteichthyes, Actinopterygii), An
478 early ray-finned fish. *Palaeontology* **58**, 849–870 (2015).
- 479 48. Grande, L. & Bemis, W. E. Osteology and Phylogenetic Relationships of Fossil and
480 Recent Paddlefishes (Polyodontidae) with Comments on the Interrelationships of
481 Acipenseriformes. *Memoir (Society of Vertebrate Paleontology)* **11 (Supplement to**
482 **Number 1)**, 1–121 (1991).
- 483 49. Eames, B. F. *et al.* Skeletogenesis in the swell shark *Cephaloscyllium ventriosum*.
484 *Journal of Anatomy* **210**, 542–554 (2007).
- 485 50. Venkatesh, B. *et al.* Elephant shark genome provides unique insights into gnathostome
486 evolution. *Nature* **505**, 174–179 (2014).
- 487 51. Ryll, B., Sanchez, S., Haitina, T., Tafforeau, P. & Ahlberg, P. E. The genome of
488 *Callorhinchus* and the fossil record: a new perspective on SCPP gene evolution in
489 gnathostomes. *Evolution & Development* **16**, 123–124 (2014).
- 490 52. Marconi, A., Hancock-Ronemus, A. & Gillis, J. A. Adult chondrogenesis and
491 spontaneous cartilage repair in the skate, *Leucoraja erinacea*. *eLife Sciences* **9**, 2813
492 (2020).
- 493 53. King, B., Qiao, T., Lee, M. S. Y., Zhu, M. & Long, J. A. Bayesian morphological
494 clock methods resurrect placoderm monophyly and reveal rapid early evolution in
495 jawed vertebrates. *Systematic Biology* **66**, 499–516 (2016).

54. Goloboff, P. A. & Catalano, S. A. TNT version 1.5, including a full implementation of phylogenetic morphometrics. *Cladistics* **32**, 221–238 (2016).
55. Ronquist, F. & Huelsenbeck, J. P. MrBayes 3: Bayesian phylogenetic inference under mixed models. *Bioinformatics* **19**, 1572–1574 (2003).
56. Clement, A. M. *et al.* Neurocranial anatomy of an enigmatic Early Devonian fish sheds light on early osteichthyan evolution. *eLife Sciences* **7**, e34349 (2018).
57. Lewis, P. O. A likelihood approach to estimating phylogeny from discrete morphological character data. *Systematic Biology* **50**, 913 (2001).
58. Rambaut, A., Drummond, A. J., Xie, D., Baele, G. & Suchard, M. A. Posterior summarization in Bayesian phylogenetics using Tracer 1.7. *Systematic Biology* **67**, 901–904 (2018).
59. R Core Team. *R: A language and environment for statistical computing*. (R Foundation for Statistical Computing, 2019).
60. Maddison, D. R. & Maddison, W. P. *Mesquite*. (2019).
61. Louca, S. & Doebeli, M. Efficient comparative phylogenetics on large trees. *Bioinformatics* **34**, 1053–1055 (2017).
62. Swofford, D. L. *PAUP**. 4.0a166, (2019).

Acknowledgements. M. Bolortsetseg generously assisted MDB with contacts and field experience in Mongolia. Fieldwork was supported by National Geographic Society grants CRE 8769-10 and GEFNE35-12 to MDB. AJ's field contributions were supported by funds from the Anna Maria Lundin's stipend from Smålands Nation, Uppsala University. RS's field contributions were supported by a Royal Society Research Grant and the University of Manchester. The majority of this work was supported by the European Research Council (ERC) under the European Union's Seventh Framework Programme (FP/2007-2013)/ERC

Grant Agreement number 311092 to MDB. RPD was also supported by the Île-de-France DIM (domaine d'intérêt majeur) matériaux anciens et patrimoniaux grant PHARE. Stig Walsh is thanked for access and loan of specimen at the National Museums of Scotland. Synchrotron tomography was performed at the ESRF (application LS 2451) with the assistance of Paul Tafforeau. SG was supported by a Royal Society Dorothy Hodgkin Research Fellowship. Matt Friedman is thanked for undertaking the X-ray computed microtomography analysis. This study includes data produced in the CTEES facility at University of Michigan, supported by the Department of Earth & Environmental Sciences and College of Literature, Science, and the Arts. TNT was made available with the support of the Willi Hennig Society.

Author Contributions: MDB conceived and designed the study. MDB, AJ, YAA, and EZ participated in all field seasons. RPD and AJ undertook preliminary CT scanning and segmentation that revealed the fossil was a 'placoderm' and had endochondral bone. RS discovered the first vertebrate remains in the first field season at Yamaat Gol in 2010. SG undertook the segmentation of *Minjinia* with input from MDB. AJ performed segmentation of *Diplacanthus* tissue. MC provided input on occipital comparative morphology of 'placoderms'. RPD provided data and comparative analyses and data for endoskeletal tissue. YAA provided background on the geology, palaeontology, and stratigraphy of the type location; EZ and YAA organized field logistics and permitting. MDB, SG, MC, RPD, and AJ undertook the anatomical interpretation and prepared the figures. MDB and SG conducted the phylogenetic analyses. RS conducted the parsimony branch support analyses. TG wrote the script for generating MrBayes partitions from TNT's character fits table and conducted the likelihood and model-fitting analyses. The manuscript was written by MDB, RPD, and SG.

546 **Competing interests statement:**

547 The authors declare no competing interests.

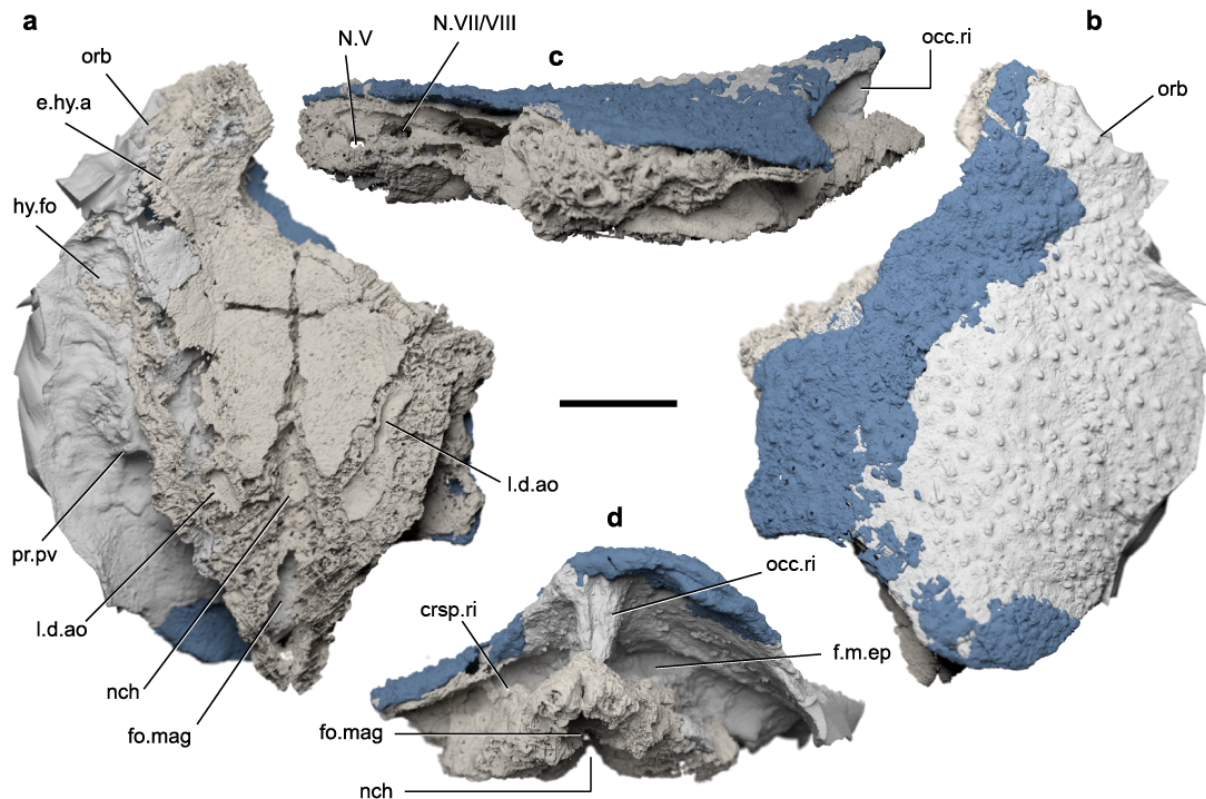


Fig. 1 | MPC-FH100/9.1 a 'placoderm' skull roof and braincase from the Early Devonian of Mongolia. **a**, Ventral view. **b**, Dorsal view. **c**, Left lateral view. **d**, Posterior view. **e**, Braincase endocavity in dorsal view. Taupe: endoskeleton; grey: mould; blue: exoskeleton. crsp.ri, craniospinal ridge; e.hy.a, sulcus for the efferent hyoid artery; f.m.ep, epaxial muscle fossa; fo.mag., foramen magnum; hy.fo, hyodean fossa; l.d.ao, sulcus for the lateral dorsal aorta; N.V, trigeminal nerve canal; N.VII, facial nerve canal; N.VIII, acoustic nerve canal; nch, notochordal canal; occ.ri, occipital ridge; orb, orbit; pr.pv, paravagal process. Scale bar, 10 mm.

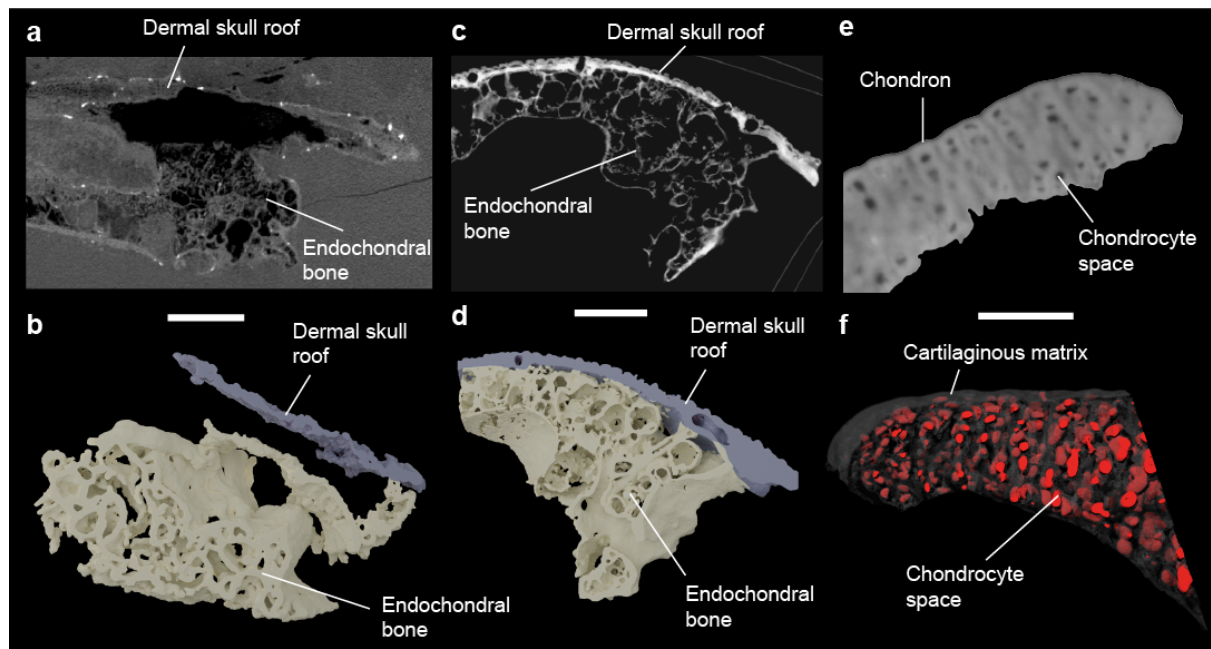


Fig. 2 | Endoskeletal mineralisation in fossil gnathostomes. **a**, Transverse tomographic slice through MPC-FH100/9.1. **b**, Three-dimensional rendering of trabecular bone structure. **c**, Transverse tomographic section through the braincase of the osteichthyan *Ligulalepis*. **d**, Three-dimensional rendering of the trabecular bone in *Ligulalepis* (**c** and **d** use data from⁵⁶). **e**, Synchrotron tomography image of the calcified cartilage of the certatohyal of the stem-group chondrichthyan *Diplacanthus crassissimus* specimen NMS 1891.92.334. **f**, Semi-transparent three-dimensional structure of calcified cartilage of NMS 1891.92.334. Scale bars, **a** and **b**, 10 mm; **c** and **d**, 1 mm; **e** and **f**, 150 µm.

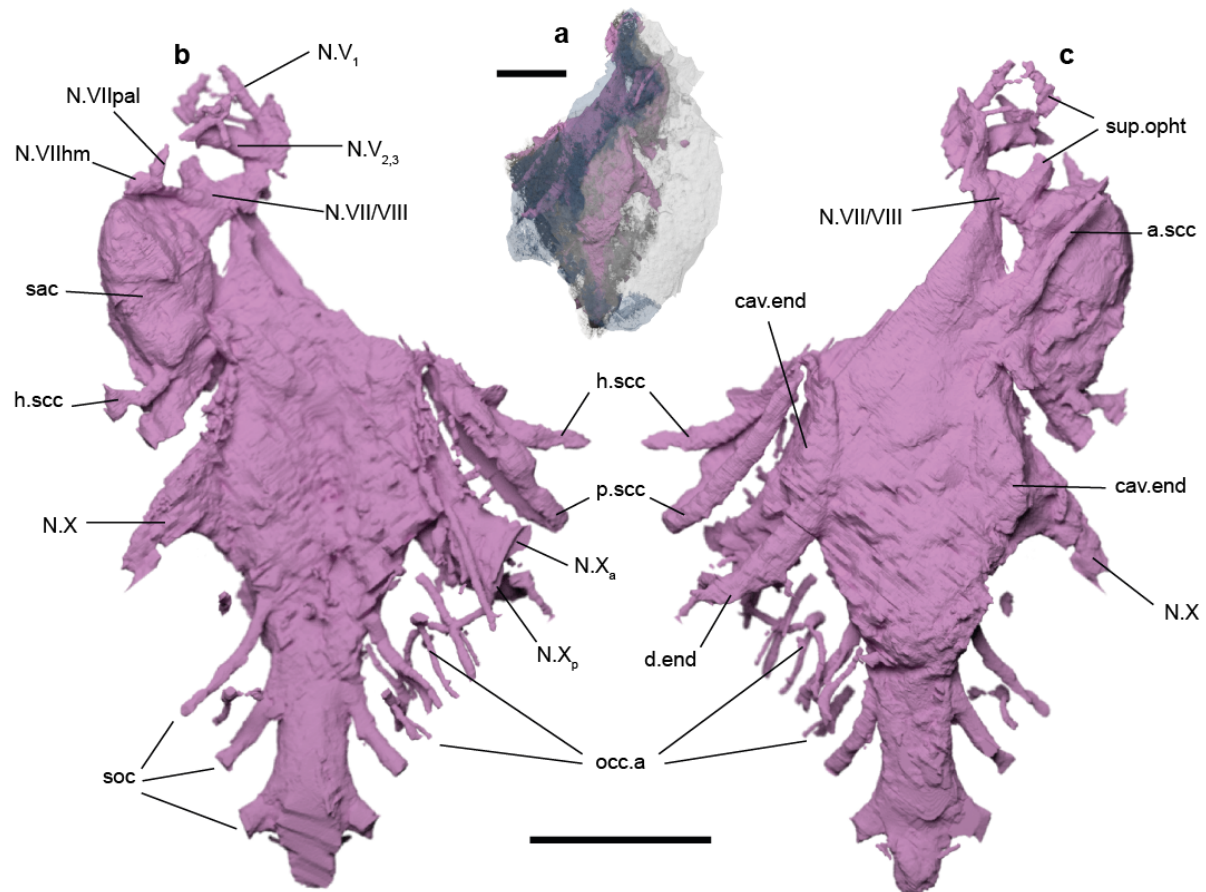


Fig. 3 | Braincase endocavity of *Minjinia*. **a**, Semi-transparent rendering of skull roof and braincase (grey and blue) showing extent of endocavity (pink). **b**, Ventral view. **c**, Dorsal view. a.scc, anterior semicircular canal; cav.end, endolymphatic cavity; d.end, endolymphatic duct; h.scc, horizontal semicircular canal; N.V, trigeminal nerve canal; N.VIIhm, hyomandibular branch of facial nerve canal; N.VIIpal, palatine branch of facial nerve canal; N.VIII, acoustic nerve canal; N.X, vagus nerve canal, N.X_a, anterior branch of vagus nerve canal; N.X_p, posterior branch of vagus nerve canal; occ.a, occipital artery canals; p.scc, posterior semicircular canal; sac, sacculus; soc, spino-occipital nerve canals; sup.opht, canal for supra-ophtalmic nerve. Scale bars, 10 mm (upper scale bar associates with **a**, lower scale bar associates with **b** and **c**).

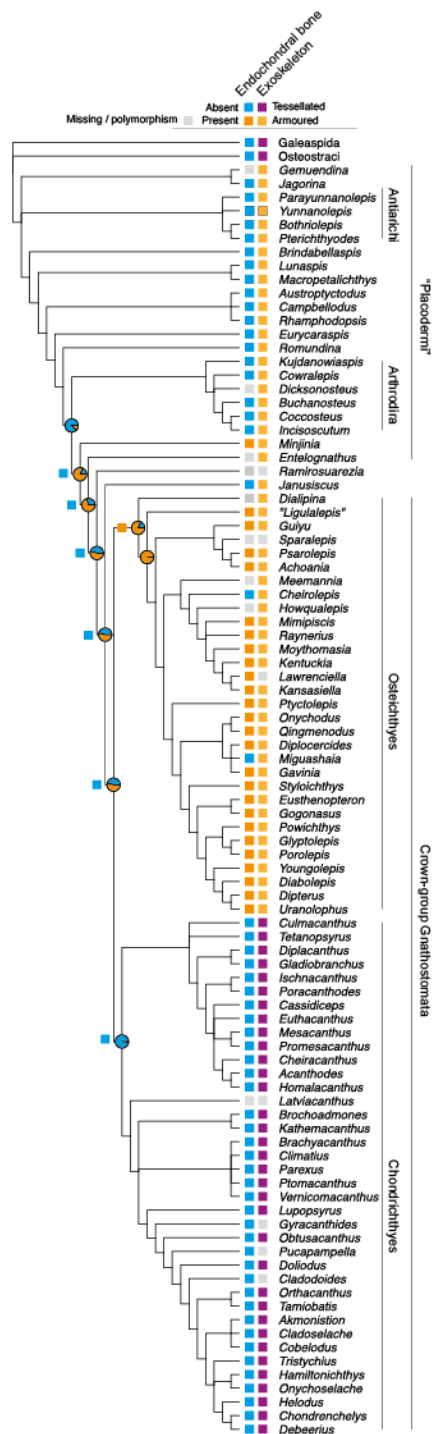
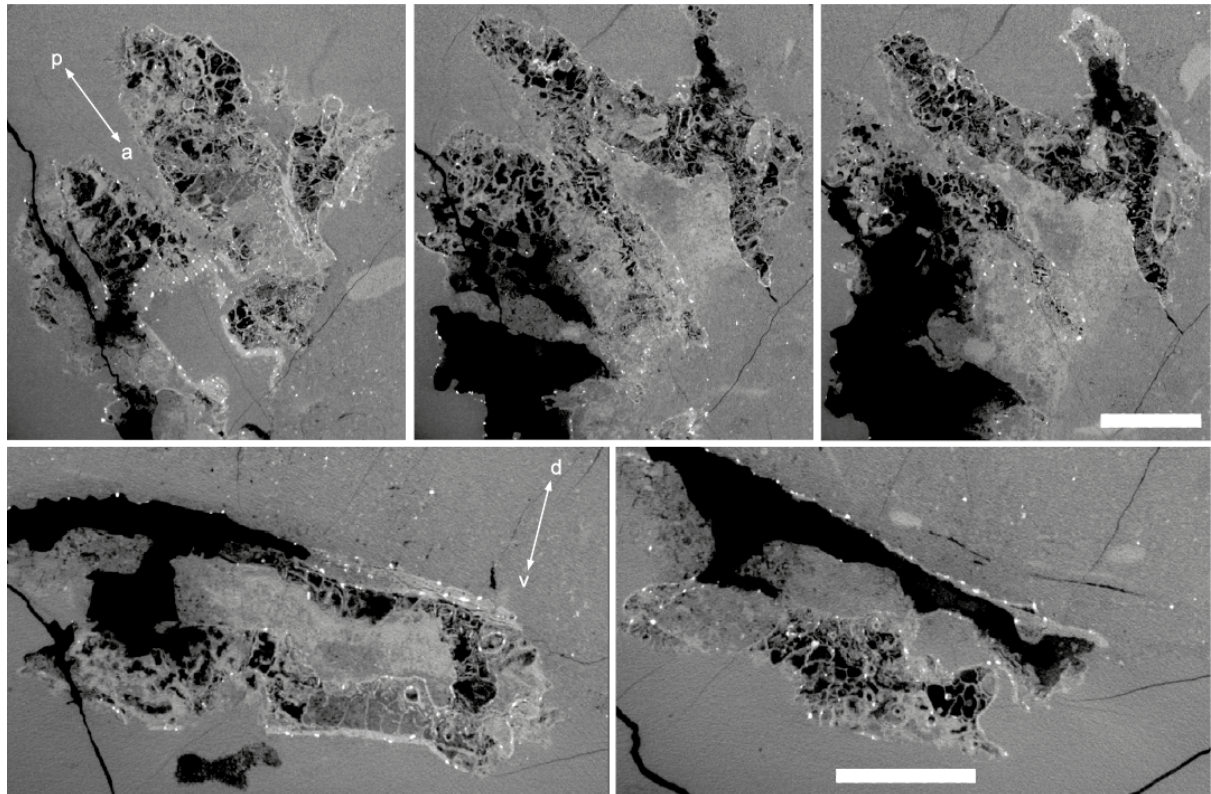


Fig. 4 | Strict consensus tree from parsimony analysis of early gnathostomes showing distribution of endochondral bone and exoskeletal armour. Squares at nodes indicate parsimony reconstruction for endochondral bone. Pie charts at nodes show likelihood reconstructions for the same character under the all-rates-different model (see Extended Data Figs 6 & 7 for competing reconstructions). Grey box indicates uncertainty. Loss of

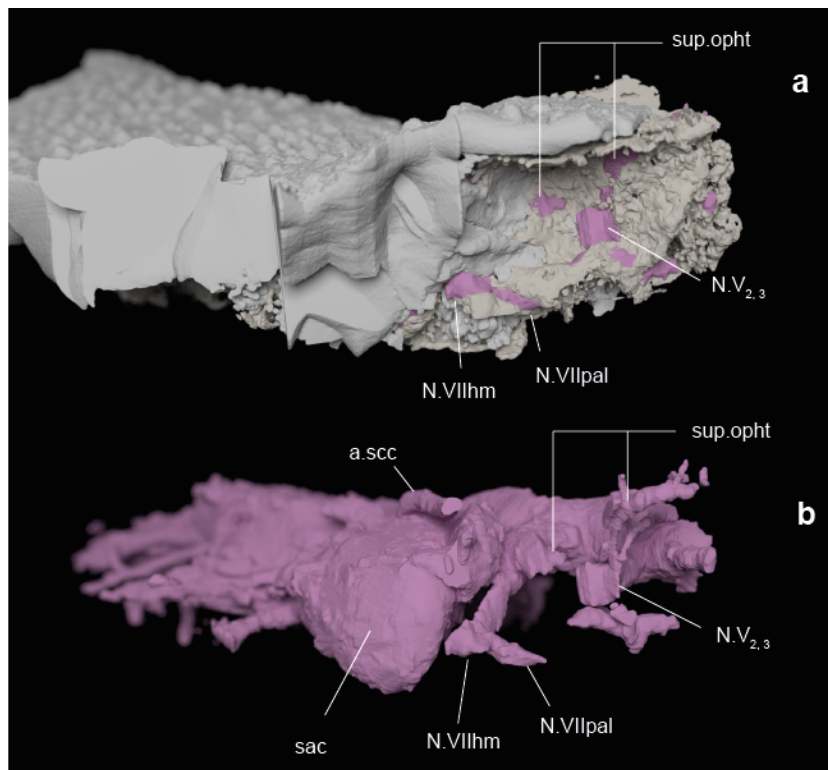
endochondral bone maps closely with generalised loss of bone in chondrichthyans where
exoskeletal armour and perichondral bone are also absent.

Table 1 | Tree distribution (n=100) ancestral states estimation results. ER = Equal rates
model; ARD = All Rates Different model. The columns AIC and log.lik represent the
median AIC and log.lik across the 100 parsimony and Bayesian trees (for both models). The
like.ratio column is the likelihood ratio for the models compared on these trees. The columns
Absent and Present represent the median scaled likelihood for the endochondral bone state.

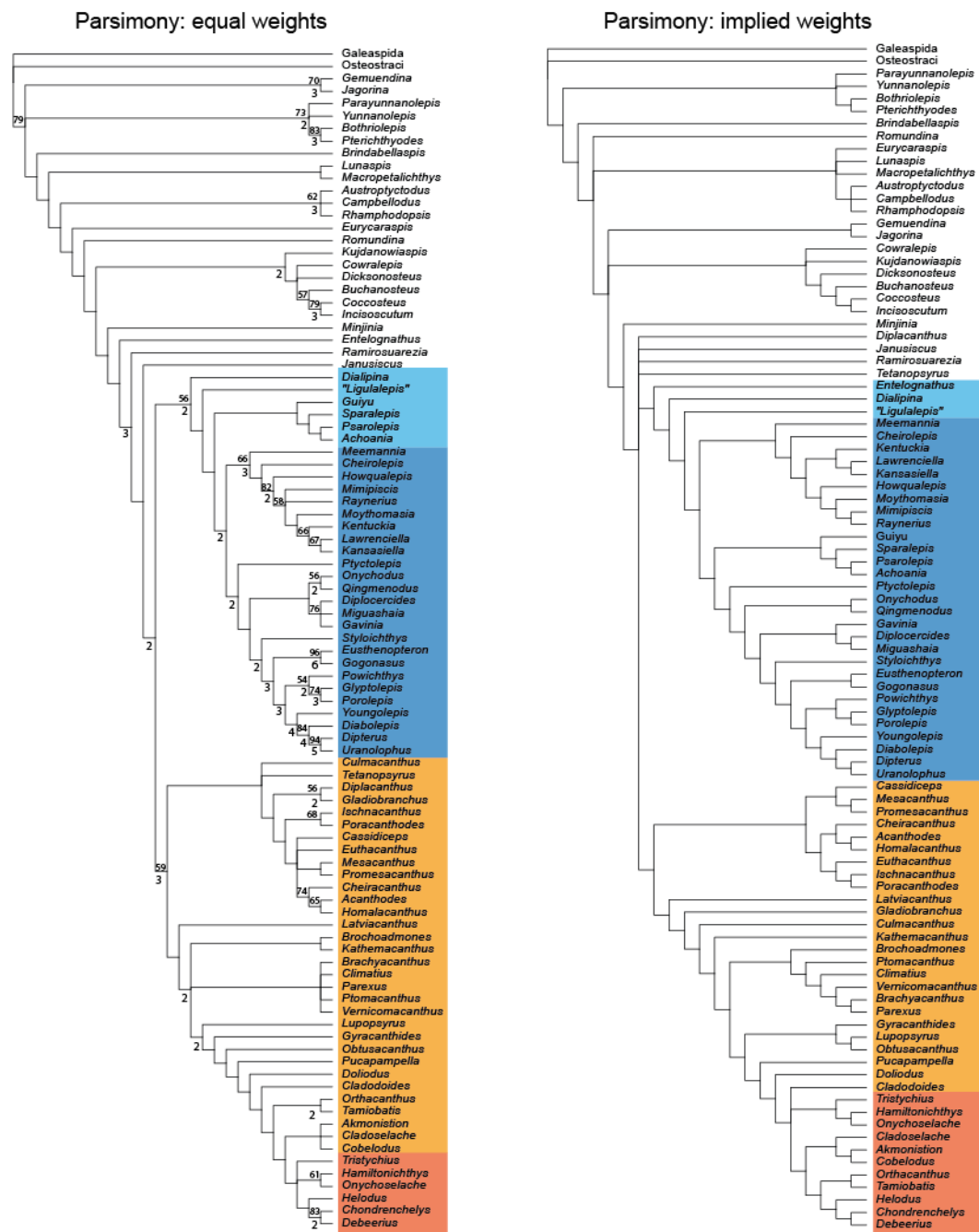
trees	model	log.lik.	like.ratio	AIC	node	Absent	Present
Parsimony (equal weights)	ER	-28.91	4.74	59.82	Minjinia:Gnathostomes	0.67	0.33
	ARD	-26.54		57.09		0.19	0.81
	ER				Crown Gnathostomes	0.91	0.09
	ARD					0.46	0.54
Bayesian (unpartitioned)	ER	-29.66	5.26	61.32	Minjinia:Gnathostomes	0.73	0.27
	ARD	-27.03		58.06		0.17	0.83
	ER				Crown Gnathostomes	0.79	0.21
	ARD					0.22	0.78



Extended Data Fig. 1 | Tomograms of endoskeletal ossification in *Minjinia*. Top row: semi-coronal sections through braincase. Double-headed arrows indicate anterior-posterior (a-p) dorsal-ventral (d-v) axes. Bottom row: semi-transverse sections through posterior part of endocranium. Voids of black space represent mouldic preservation. Scale bars, 10 mm and apply across each row of panels.



Extended Data Fig. 2 | Right orbital wall and innervation pattern of *Minjinia*. **a**, orbit in anterolateral view showing disposition of nerve openings (pink infill). **b**, endocast in the same perspective showing the relationship between nerve canals and endocast. a.scc., anterior semicircular canal; N.V_{2,3} trunk of the trigeminal nerve canal for branches 2 and 3; N.VII_{hm}, hyomandibular branch of facial nerve canal; N.VII_{pal}, palatine branch of facial nerve canal; sac., sacculus; sup.opht, canal for supra-ophtalmic nerve. Scale bars, 20 mm (upper scale bar associates with **a**, lower scale bar associates with **b** and **c**).

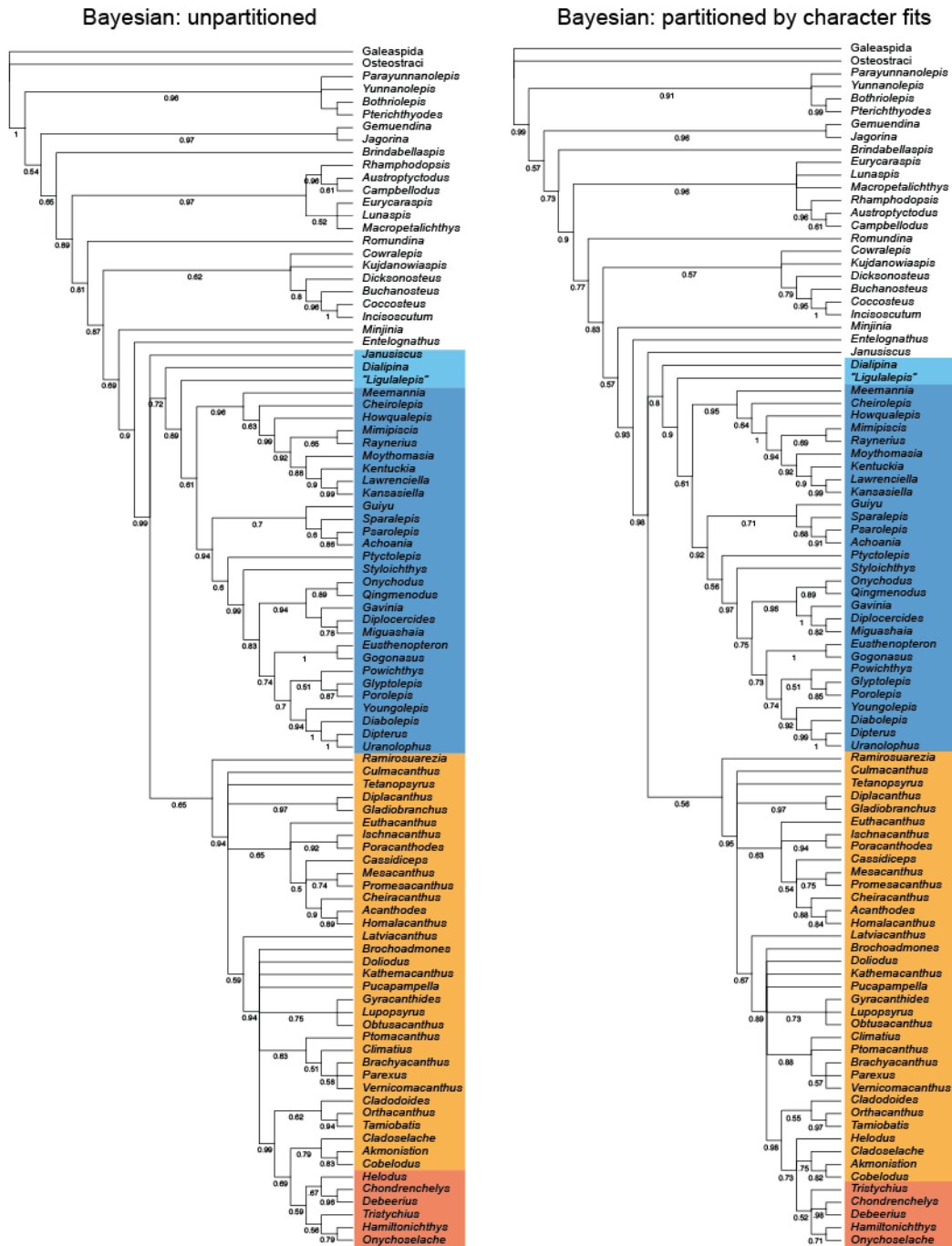


611

612 **Extended Data Fig. 3 | Results of phylogenetic parsimony analysis.** Dataset consists of 95
 613 taxa and 284 characters. Both trees are strict consensus topologies. Equal weights parsimony
 614 analysis using the ratchet resulted in 240 trees with a length of 831 steps. Implied weights
 615 parsimony analysis using random addition sequence + branch-swapping resulted in 8 optimal
 616 trees with score 85.20513. Double-digit figures above internal branches are bootstrap values
 617 of 50% and over; single-digit figures below branches are Bremer decay index values. Blue

618 shading: osteichthyan total group (dark blue: crown group); orange shading: chondrichthyan
619 total group (dark orange: crown group).

620



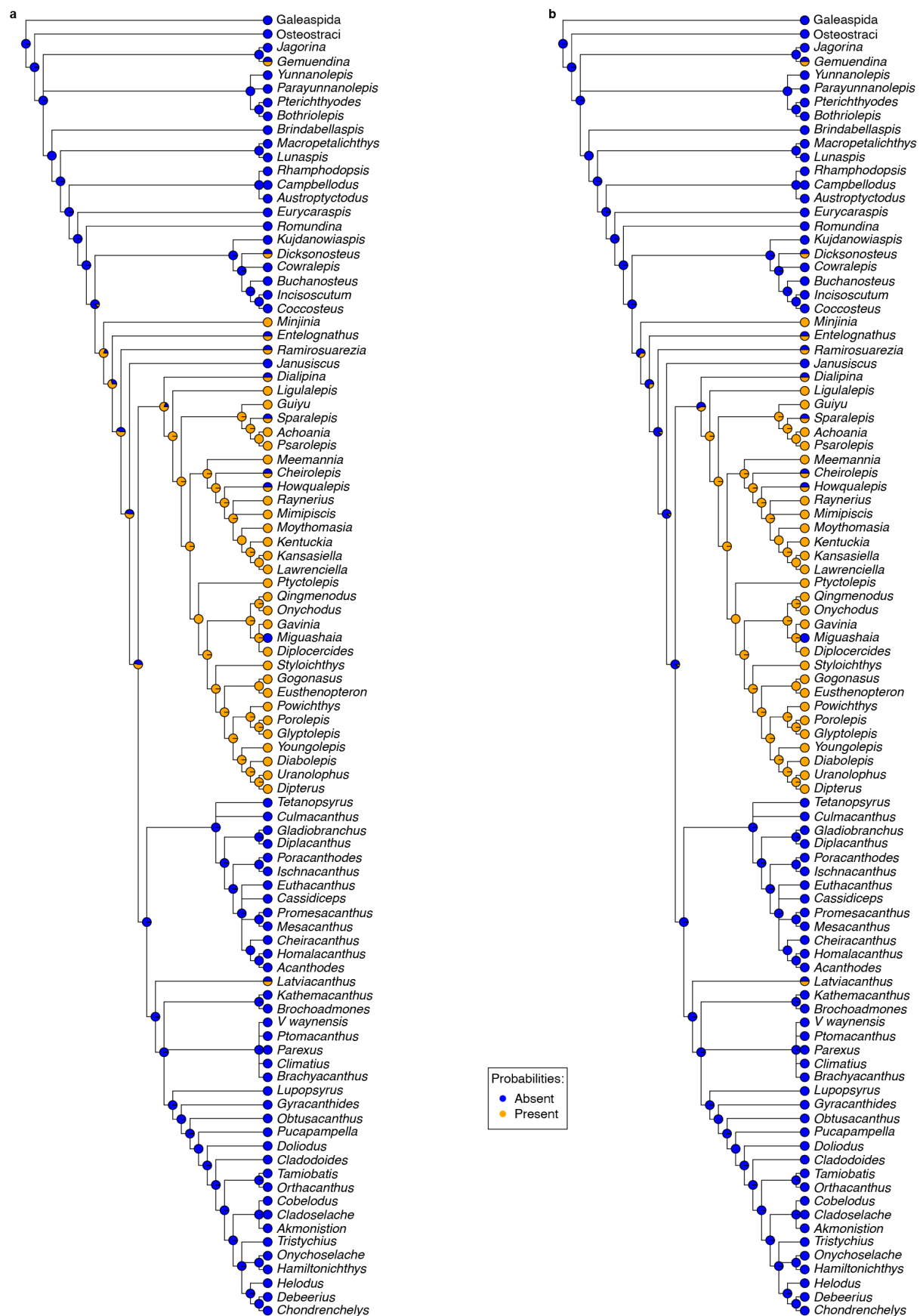
621

622 **Extended Data Fig. 4 | Results of Bayesian phylogenetic analysis using both partitioned**

623 **and unpartitioned data. Majority-rules consensus trees with posterior probabilities shown**

624 along branches. Blue shading: osteichthyan total group (dark blue: crown group); orange
625 shading: chondrichthyan total group (dark orange: crown group).

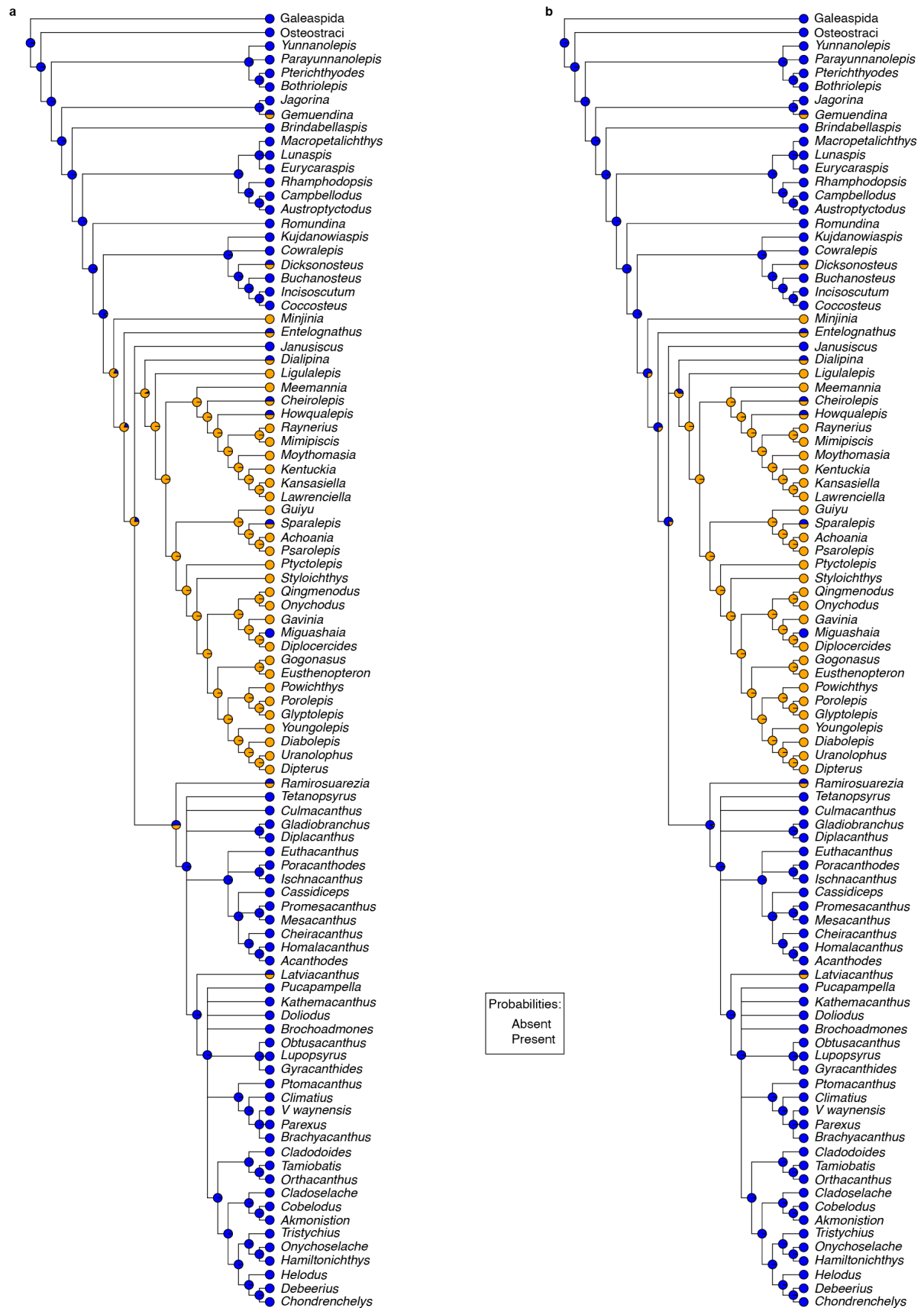
626



629 **equal weights parsimony results. a**, ARD, all rates different model; **b**, ER, equal rates

630 model.

631



632

633 Extended Data Fig. 6 | Likelihood ancestral state mapping of endochondral bone on

634 **unpartitioned Bayesian analysis results. a**, ARD, all rates different model; **b**, ER, equal
635 rates model.